Extreme Nonreciprocal Near-Field Thermal Radiation via Floquet Photonics

Lucas J. Fernández-Alcázar, Rodion Kononchuk, Huanan Li, and Tsampikos Kottos

Phys. Rev. Lett. **126**, 204101 — Published 21 May 2021

DOI: 10.1103/PhysRevLett.126.204101

Extreme Non-Reciprocal Near-Field Thermal Radiation via Floquet Photonics

Lucas J. Fernández-Alcázar[1], Rodion Kononchuk[1], Huanan Li[2], Tsampikos Kottos[1]
[1] *Wave Transport in Complex Systems Lab, Department of Physics, Wesleyan University, Middletown, CT-06459, USA*
[2] *Photonics Initiative, Advanced Science Research Center, CUNY, NY 10031, USA*
(Dated: April 16, 2021)

By utilizing Floquet driving protocols and interlacing them with a judicious reservoir emission engineering we achieve extreme non-reciprocal thermal radiation. We show that the latter is rooted in an interplay between a direct radiation process occurring due to temperature bias between two thermal baths and the modulation process which is responsible for pumped radiation heat. Our theoretical results are confirmed via time-domain simulations with photonic and RF circuits.

Introduction - Thermal radiation is associated with the conversion of the thermal motion of (quasi-)particles, in matter with some finite temperature, into electromagnetic emission. Its management constitutes a major challenge with both fundamental and technological ramifications [1–8]. For example, some of the ongoing investigations aim to establish paradigms that challenge fundamental limitations in thermal radiation, set by Kirchhoff's emissivity-absorptivity equivalence law [9–13] and by Planck's upper bound of thermal emission [14–17]. In parallel, other studies exploit the applicability of recent proposals for radiation control to daytime passive radiative cooling [18–22], radiative cooling of solar cells [23–25], energy harvesting [26–33], thermal camouflage [34, 35], etc. It turns out that the implementation of subwavelength photonic circuits reinforces the importance of evanescent waves in radiation and allows us to bypass the constraints set by Kirchoff's and Planck's laws. This symbiosis of nanophotonics and thermal radiation led to the establishment of thermal photonics, which holds promises for novel technologies in energy harvesting and near-field thermal radiation management [36, 37].

A long-standing problem in thermal radiation management is the quest for novel non-reciprocal (NR) devices that control the directionality of photon emissivity. Along these lines, researchers have proposed a variety of schemes ranging from magneto-optical effects [39–42] to non-linearities [43–46] and active photonic circuits [47–49] for enforcing directional thermal radiation.

Here we unveil an interplay between three elements that control the efficiency of thermal rectification in Floquet-driven circuits: (a) a judiciously engineered bath emissivity (via photonic filters) of the thermal reservoirs; (b) an appropriately designed Floquet protocol that enforces a time modulation of the constituent parameters of a photonic circuit; and (c) the temperature gradient between two thermal reservoirs which are coupled resonantly with the circuit. The latter is responsible for a biased current while the second element is generating pumped thermal radiation which can balance the biased thermal current in one specific direction leading to high rectification. In fact, for moderate driving frequencies we are able to achieve perfect rectification and even refrigeration. We utilize these elements for the design of optimal reconfigurable Floquet-based thermal diodes and validate the theoretical predictions via time-domain simulations.

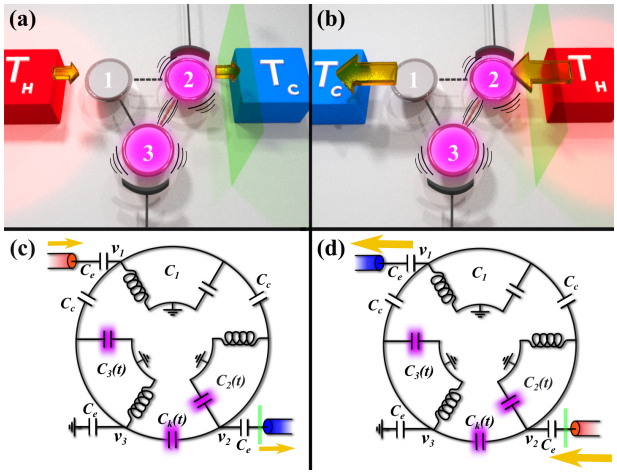

FIG. 1: A photonic Floquet diode for near-field thermal radiation. The resonators $n = 2, 3$ and the coupling between them are periodically modulated in time while the $n = 1$-resonator is static: (a) In the "forward" (f) configuration, the reservoir with the high (low) temperature $T_{\alpha=1} = T_H$ ($T_{\alpha=2} = T_C$) is coupled to the $n = 1 (n = 2)$-resonator. (b) In the "backward" (b) configuration the low (high) temperature reservoir $T_{\alpha=1} = T_C (T_{\alpha=2} = T_H)$ is coupled to the $n = 1 (n = 2)$-resonator. An equivalent electronic circuit. The LC resonators $n = 2, 3$ and their coupling are driven by modulating the (pink) capacitors: (c) Forward and (d) Backward configurations. The currents are measured at the same position at the $\alpha = 2$ transmission line (green transparent plane in (a-b); bold green line in (c-d)).

Coupled-Mode-Theory – We consider a photonic network of N coupled modes. The field dynamics in such a network is described by a time-dependent effective coupled-mode-theory (CMT) Hamiltonian $H_0(t) = H_0(t + \frac{2\pi}{\Omega})$. Two of these modes are connected directly to two reservoirs at temperatures $T_{\alpha=1} \neq T_{\alpha=2}$, see Fig. 1, that emit a mean number of photons $\Theta_\alpha(\omega) = \{\exp[\hbar\omega/(k_B T_\alpha)] - 1\}^{-1}$ at frequency ω. We study the radiative energy transfer between these reservoirs for a

forward (Fig. 1a) and a backward (Fig. 1b) configuration. The process is modeled by a temporal-CMT [50, 51]

$$\begin{aligned} -\imath\frac{d\left|\psi(t)\right\rangle}{dt} &= H_{\text{eff}}\left|\psi(t)\right\rangle - \imath D^T\left|S^+(t)\right\rangle;\ H_{\text{eff}} = H_0(t) + \imath\Gamma \\ \left|S^-\right\rangle &= -\left|S^+\right\rangle + D\left|\psi\right\rangle, \end{aligned} \quad (1)$$

where the amplitudes $|\psi\rangle = (\psi_1, \cdots, \psi_N)^T$ are normalized such that $|\psi_n|^2$ represents the energy in the $n = 1, \cdots, N$-th mode. The matrix $\Gamma_{nm} = \gamma_\alpha \delta_{n,\alpha}\delta_{nm} + \Sigma_{nm}(t)$ represents the dissipation of the n-th mode. Here, $\Sigma_{nm}(t)$ describes driving-induced losses and/or gain and γ_α is the dissipation due to coupling of the $n-$th mode with the reservoir α. From the fluctuation-dissipation relation, we also have that $D_{n,\alpha} = \sqrt{2\gamma_\alpha}\delta_{n,\alpha}$. Finally, $S^\pm_\alpha(t) = \int_0^\infty S^\pm_\alpha(\omega)e^{\imath\omega t}d\omega$ indicate the incoming (+) and outgoing (−) thermal excitations from and towards the α-th reservoir. The amplitudes $S^+_\alpha(\omega)$ satisfy the relation

$$\left\langle [S^+_{\alpha'}(\omega')]^* S^+_\alpha(\omega)\right\rangle = \frac{\hbar\omega}{2\pi}\phi_\alpha(\omega)\Theta_\alpha(\omega)\delta(\omega-\omega')\delta_{\alpha,\alpha'}, \quad (2)$$

where $\phi_\alpha(\omega)$ describes spectral filtering of the $\alpha-$th thermal reservoir. Existing proposals for the control of spectral emissivity of the thermal reservoirs include the deposition of photonic crystals that support band-gaps, or their coupling to the photonic circuit via a waveguide or a cavity with cut-off frequencies, etc. [5–7].

Floquet Scattering for Thermal Radiation– In Floquet scattering, an incident excitation $S^+_\alpha(\omega)$ at frequency ω can change its frequency by $\pm l\Omega$ and scatter out of the modulated target at a Floquet channel $\omega_l = \omega + l\Omega$ where $l \in (-\infty, \cdots, \infty)$. The Floquet scattering matrix $\mathcal{S}^F$, connecting the outgoing to the incoming field amplitudes $\vec{S}^\pm = [\cdots, |S_\pm(\omega_{+1})\rangle, |S_\pm(\omega_0)\rangle, |S_\pm(\omega_{-1})\rangle, \cdots]^T$, is evaluated using Eq. (1)

$$\mathcal{S}^F = -I - \imath[D]G^F[D]^T; \quad G^F = \left(\omega I - \hat{H}_Q\right)^{-1}, \quad (3)$$

where $[D]$ represents a block diagonal matrix with blocks D, and G^F is the Green's function associated with the Floquet Hamiltonian $\hat{H}_Q$. The latter takes the form $\langle l, n|\hat{H}_Q|l', n'\rangle = \frac{\Omega}{2\pi}\int_0^{\frac{2\pi}{\Omega}} dt e^{-\imath(l'-l)\Omega t}[H_{\text{eff}}(t)]_{n,n'} - l\Omega\delta_{l,l'}\delta_{n,n'}$ [52–55]. Using Eq. (3) we have calculated the average energy current $\bar{I}_\alpha$ entering reservoir α [56]

$$\bar{I}_\alpha = \int \frac{d\omega}{2\pi}\sum_\beta \mathcal{T}^F_{\alpha,\beta}(\omega)\left[\hbar\omega\phi_\beta(\omega)\Theta_\beta(\omega)\right], \quad (4)$$

where $\mathcal{T}^F_{\alpha,\beta}(\omega) = \sum_l\left(-\delta_{\alpha,\beta}\delta_{l,0} + \left|\mathcal{S}^F_{\alpha,\beta}(\omega_l,\omega)\right|^2\right)$ is the total transmittance of radiation entering the $\alpha-$th reservoir at frequencies ω_l provided that it was emitted at reservoir β at frequency ω. A positive value of $\bar{I}_\alpha$ indicates that current flows toward the α-th heat bath.

Equations (3,4) extend the standard treatment of thermal radiation to periodically modulated photonic circuits and provide a bridge with the field of Floquet engineering [55, 57, 58]. It turns out that time-dependent perturbations could induce NR transmittance $\mathcal{T}^F_{\alpha,\beta}(\omega) \neq \mathcal{T}^F_{\beta,\alpha}(\omega)$ [59–61] whose origin is traced to interference effects between different paths in the Floquet ladder [55]. At the same time, Eqs. (3,4) emphasize the fact that while NR transmittances $\mathcal{T}^F_{\alpha,\beta}(\omega) \neq \mathcal{T}^F_{\beta,\alpha}(\omega)$ are a necessary condition, they are not sufficient for establishing NR thermal radiation. In fact, integrating over frequencies with a weight $\phi_{\alpha/\beta}(\omega)\Theta_{\alpha/\beta}(\omega)$ might suppress the NR heat flux. Let us finally point out that a key characteristic of time-modulated NR schemes is their power consumption. The latter is determined by the same factors as in optical modulators [61] where recent strategies led to its dramatic reduction up to fraction of a nW [62].

Rectification Efficiency - We consider three single-mode resonators $n = 1, 2, 3$, equally coupled with one another, see Figs. 1a,b. The first and the second resonators are at the proximity of two reservoirs with temperatures $T_H > T_C$. We compare the emitted energy flux $\bar{I}_\alpha$ at a reference reservoir (e.g. $\alpha = 2$) for two different configurations: (i) The forward (f) configuration where the cavity $n = 1$ is in the proximity of the hot reservoir i.e. $T_{\alpha=1} = T_H$ and the cavity $n = 2$ is coupled to a cold reservoir i.e. $T_{\alpha=2} = T_C < T_H$ (see Fig. 1a). (ii) The backward (b) configuration (see Fig. 1b) where $T_1 = T_C < T_H = T_2$. The NR efficiency is described by the rectification parameter $\mathcal{R}$

$$\mathcal{R} \equiv \frac{\bar{I}^{(f)}_2 - (-\bar{I}^{(b)}_2)}{\bar{I}^{(f)}_2 + (-\bar{I}^{(b)}_2)}, \quad (5)$$

where $\mathcal{R} = \pm 1$ indicates perfect diode action, while $\mathcal{R} = 0$ corresponds to completely reciprocal radiation. A rectification parameter $|\mathcal{R}| > 1$ indicates that the photonic circuit operates as a "refrigerator". We will assume that T_C is fixed. A qualitative understanding of the effects of a temperature gradient $\Delta T \equiv T_H - T_C$, modulation frequency Ω, and spectral filtering $\phi(\omega)$ on $\mathcal{R}$, is achieved by analyzing the slow driving limit $\Omega \to 0$. Below we will assume that the scattering process in the absense of driving $\Omega = 0$ is always reciprocal.

In the forward configuration, the current Eq. (4) is approximated as the sum of two contributions [38, 56]

$$\bar{I}^{(f)}_2 \approx \bar{I}^{(f)}_{2,b} + \bar{I}^{(f)}_{2,p}, \quad (6)$$

where $\bar{I}^{(f)}_{2,b}$ is the current due to temperature bias and $\bar{I}^{(f)}_{2,p}$ is a pumped current associated with the time modulation of the circuit [47]. Further progress is made by considering the classical limit ($\phi_\beta \equiv 1$, $\Theta_\beta(\omega) \approx \frac{k_B T_\beta}{\hbar\omega}$) where

$$\begin{aligned} \bar{I}^{(f)}_{2,b} &\approx \hat{\mathcal{T}}\ k_B(T_1 - T_2), \quad \hat{\mathcal{T}} = \int \frac{d\omega}{2\pi}\bar{\mathcal{T}}(\omega); \quad (7) \\ \bar{I}^{(f)}_{2,p} &\approx \frac{\Omega}{2\pi}\hat{\mathcal{P}}\ k_B T_0; \hat{\mathcal{P}} = \int \frac{d\omega}{2\pi}\frac{\imath}{\omega}\int_0^{\frac{2\pi}{\Omega}} dt\left(\frac{dS^t}{dt}(S^t)^\dagger\right)_{2,2}, \end{aligned}$$

where $T_0 = \frac{T_1+T_2}{2}$ and the averaged (over one modulation cycle) transmittance $\bar{\mathcal{T}}(\omega) = \frac{\Omega}{2\pi}\int dt|S^t_{21}(\omega)|^2$ can be evaluated using the instantaneous scattering matrix $S^t = -I_2 - DGD^T$, with $G = \left[\omega I_N - (H^t_0 + \imath D^T D/2)\right]^{-1}$, H^t_0 the Hamiltonian $H_0(t)$ evaluated at specific time t and I_m the $m \times m$ identity matrix. Equations (7) are valid for $\Omega, \Delta T/T_0 \to 0$. Notice that $\bar{I}^{(f)}_{2,p}$ is proportional to Ω but independent of ΔT.

Following the same analysis, we evaluate $\bar{I}^{(b)}_2$. Its bias component is $\bar{I}^{(b)}_{2,b} = -\bar{I}^{(f)}_{2,b}$ while the pumping current is $\bar{I}^{(f)}_{2,p} \approx \bar{I}^{(b)}_{2,p}$. It is, therefore, possible to find parameters $(\Delta T^*, \Omega^*)$ for perfect diode operation $|\mathcal{R}(\Delta T^*, \Omega^*)| \approx 1$ by imposing current in the forward (backward) configuration $\bar{I}^{(f)}_2 \approx 0 (\bar{I}^{(b)}_2 \approx 0)$ while at the same time $\bar{I}^{(b)}_2 \neq 0 (\bar{I}^{(f)}_2 \neq 0)$. Substituting in Eq. (5) the results for $\bar{I}^{(f/b)}_2$, we find

$$\mathcal{R}(\Delta T, \Omega) \approx \frac{\hat{\mathcal{P}}}{\hat{\mathcal{T}}} \frac{\Omega/(2\pi)}{(\Delta T/T_0)} \tag{8}$$

indicating that thermal rectification increases proportionally to Ω and inversely proportional to ΔT. The former is responsible for inducing NR transport $\mathcal{T}^F_{\alpha,\beta}(\omega) \neq \mathcal{T}^F_{\beta,\alpha}(\omega)$ and a pumped current, while the latter controls the bias current. From Eq. (8) we conclude that $\mathcal{R}$ is enhanced by reducing the weighted instantaneous transmittance $\hat{\mathcal{T}}$. This is achieved by confining the frequency integration in Eq. (7) via a filtering function $\phi(\omega)$. Of course, the filtering process must maintain the frequency range for which the Floquet transmittance is non-reciprocal.

CMT modeling– We consider the photonic circuit of Figs. 1a,b described by the effective Hamiltonian H_0

$$H_0 = \begin{pmatrix} \omega_1 & k_{12} & k_{13} \\ k_{21} & \omega_2 & k_{23} \\ k_{31} & k_{32} & \omega_3 \end{pmatrix} \tag{9}$$

where $k_{nm} = k_{mn} = k$ is the evanescent coupling between the resonators. In the absence of any modulation $\omega_n = \omega_0$, and due to rotational symmetry, the system has two degenerate right/left- handed modes $(1, e^{\pm 2i\pi/3}, e^{\pm 4i\pi/3})^T/\sqrt{3}$ with frequency $\omega_{L(R)} = \omega_0 - k$ and a mode $(1,1,1)^T/\sqrt{3}$ with frequency $\omega_C = \omega_0 + 2k$.

The situation is different in the presence of periodic modulations [59–61]. Guided by previous Floquet engineering studies, we implement a driving protocol that establishes a Floquet lattice with loops consisting of a sequence of directed and directionless bonds between its sites; thus inducing interferences that eventually lead to NR transport [57, 58]. In our example we modulate the $n = 2, 3$- resonators with $\omega_n = \omega_0 - \delta_0\left[\cos(\Omega t + \phi_n) + \cos(\Omega t + \phi_0)\right]$, combined with the driving of the coupling constant $k_{23} = k_{32} = k + \delta_0 \cos(\Omega t + \phi_0)$ while $n = 1$-resonator remains undriven, i.e. $\omega_1 = \omega_0$. In this case, the degeneracy of the two counter-rotating modes is lifted due to angular momentum biasing induced by the driving [59] and the transmittance demonstrates a pronounced NR behavior $\mathcal{T}^F_{1,2} \neq \mathcal{T}^F_{2,1}$ around $\omega \approx \omega_{L(R)}$ that is maximized by an appropriate choice of the phasors $\phi_0 = 0$, $\phi_2 = +\pi/2$, and $\phi_3 = -\pi/2$ (see Fig. 2a) [58]. Finally, the modulated coupling introduces an extra non-diagonal element in the dissipation matrix Γ which becomes $\Gamma_{nm} = (\gamma_\alpha \delta_{n,\alpha} - 2\dot{\omega}_n(t)/\omega_0)\delta_{n,m} - (2\dot{k}(t)/\omega_0)(\delta_{n,2}\delta_{m,3} + \delta_{n,3}\delta_{m,2})$, with $\gamma_3 = 0$.

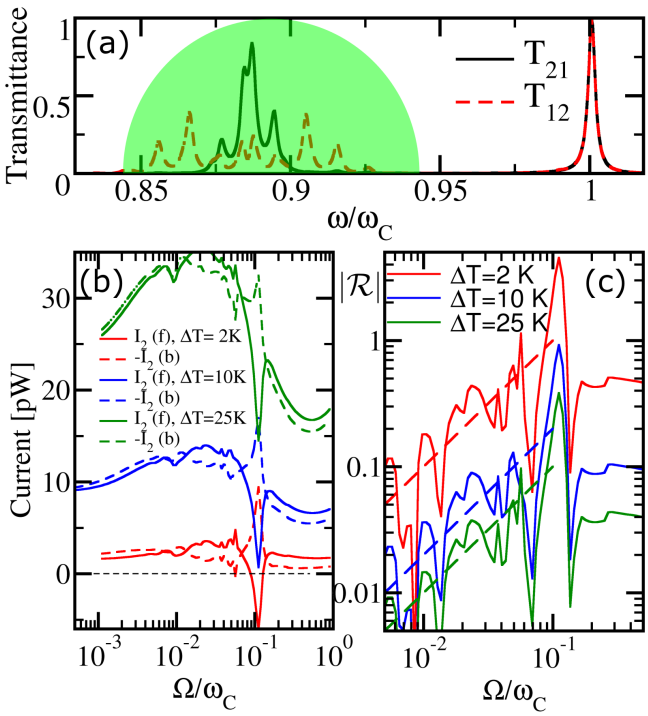

FIG. 2: (a) Transmittance spectrum $\mathcal{T}^F_{\alpha,\beta}(\omega)$ for the photonic circuit of Eq. (9) showing a nonreciprocal behavior around $\omega \sim 0.88\omega_C$. Parameters: $\Omega = 0.01\omega_C, k = 0.04\omega_C, \delta_0 = 0.015\omega_C, \gamma_1 = \gamma_2 \approx 0.004\omega_C, \gamma_3 = 0, \omega_C \approx 190{\times}10^{12}\ rad\ s^{-1}$, $T_C = T_H - \Delta T = 300$K. The green area describes the engineered emission spectrum, Eq. (10). (b) The radiative currents Eq. (4) vs. Ω for three representative temperature gradients ΔT. (c) The rectification parameter $|\mathcal{R}|$ vs. Ω. The dashed lines represent the function $R = (\alpha/\Delta T) \times \Omega$ with $\alpha = 20$ from a best fit.

In Fig. 2b, we report the currents $\bar{I}^{(f/b)}_{\alpha=2}$ calculated using Eq. (4) for three different temperature gradients ΔT. We observe that as Ω increases, the radiated current becomes non-reciprocal $\bar{I}^{(f)}_2 \neq -\bar{I}^{(b)}_2$. The associated rectification parameter $\mathcal{R}$ is shown in Fig. 2c. We find that for small Ω it agrees with Eq. (8).

For temperature gradients $\Delta T^* < 10K$, one can achieve perfect isolation in the forward configuration i.e. $I^{(f)}_2 = 0$ while $\bar{I}^{(b)}_2 \neq 0$. Specifically, at $\Delta T^* = 10K$, the associated driving frequency for which the bias current in the forward configuration balances the pumped

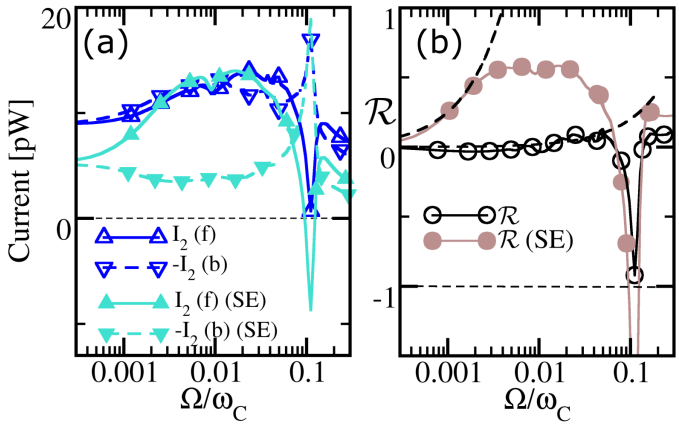

FIG. 3: (a) The currents Eq. (4) vs. Ω are calculated with (filled symbols) and without (open symbols) spectral engineering (SE) for a forward/backward $\bar{I}_2^{(f/b)}$ configuration. (b) The rectification $\mathcal{R}$ vs. Ω for temperature gradient $\Delta T = 10K$. Other parameters are as in Fig. 2. The black dashed lines indicate a function $R = \alpha \times \Omega$ with best fitting values $\alpha = 2$ (250) for the unfiltered (filtered) circuit.

current is $\Omega^* \approx \omega_C - \omega_{L(R)} \approx 3k$. The latter corresponds to a resonant driving that promotes transitions between the frequency domain around $\omega \approx \omega_C$, where transport is reciprocal $\mathcal{T}_{12}^F = \mathcal{T}_{21}^F$, and the domain $\omega \approx \omega_{L/R}$ where $\mathcal{T}_{12}^F \neq \mathcal{T}_{21}^F$. For smaller $\Delta T = 2K$ and $\Omega^* = 3k$, the biased current in the forward configuration $\bar{I}_{2,b}^{(f)} \sim \Delta T$ is smaller (in magnitude) than the pumped current $\bar{I}_{2,p}^{(f)} \sim \Omega$, thus leading to a total emitted radiation from the cold reservoir i.e. the circuit operates as a "refrigerator" with $|\mathcal{R}| > 1$, see Fig. 3.

Next, we engineered the emission spectrum in a way that it excludes the reciprocal frequency range around $\omega \approx \omega_C$ and enforces emission in the range where nonreciprocity is maximum. To this end, we incorporated in Eq. (2) the filtering function

$$\phi(\omega) = \Re\left\{\sqrt{1 - [(\omega - \omega^*)/(b\omega_C)]^2}\right\} \tag{10}$$

with spectral width $b = 0.05$ and $\omega^*/\omega_C \approx 0.88$ being the frequency around which the transmittance is nonreciprocal. In Figs. 3a,b we report the radiative currents and rectification $\mathcal{R}(\Omega)$ for $\Delta T = 10K$. Comparison with the unfiltered reservoirs $\phi(\omega) = 1$ indicates that the spectrally engineered reservoirs lead to a superior rectification. As in the unfiltered case, also here the rectification $\mathcal{R} \sim \Omega$ in the small Ω-regime – albeit the linear coefficient is much larger (see dashed lines), in agreement with the expectations from Eq. (8).

We have also confirmed the CMT results by analyzing photonic structures consisting of time-modulated whispering gallery mode resonators. The details of these simulations are given in the Supplement.

Electronic Circuit Implementation - We further validated our results via time-domain simulations for a realistic electronic circuit (Figs. 1c,d)[56, 63]. The circuit consists of three LC resonators, with identical (and constant) inductances L. Modulation in the frequency of the $n = 2, 3$ LC resonators is achieved by changing their capacitances as $C_n(t) = C[1 + \delta\cos(\Omega t + \varphi_n)]$. The LC elements are capacitively coupled with capacitances $C_c = \kappa C$. The two time-modulated resonators are coupled via a modulated capacitance $C_\kappa(t) = C[\kappa + \delta\cos(\Omega t + \phi_0)]$. Each (undriven) resonator supports one resonant mode with frequency $\omega_0 = 1/\sqrt{LC} = 2\pi 10^9 rad/s$, and resonance impedance $z_0 = \sqrt{L/C} = 70\text{Ohms}$.

The time-dependent voltages at the connection nodes of each resonator $v_\alpha(t)$ are driven by synthesized noise sources attached to transmission lines (TLs) which are connected to each nodal point. The TLs are introduced through their Thevenin equivalent TEM transmission lines with characteristic impedance $Z_0 = 50Ohms$. They are coupled to the resonators through small capacitances $C_e = \epsilon C$. The noise sources V_α are synthesized such that

$$\langle V_{\alpha'}(\omega) V_\alpha^*(\omega')\rangle = \frac{2Z_0}{\pi}\phi_\alpha(\omega)\hbar\omega\Theta_\alpha(\omega)\delta(\omega - \omega')\delta_{\alpha,\alpha'} \tag{11}$$

where $\Theta_\alpha(\omega) = k_B T_\alpha$ is evaluated at its classical limit and $\phi_\alpha(\omega) = \phi(\omega)$ describes a filtering function.

The net energy current flowing to a transmission line α is evaluated from the time-dependent voltages $v_\alpha(t)$ and currents $i_\alpha(t)$ at the respective nodes,

$$\bar{I}_\alpha = \int d\omega \bar{I}_\alpha(\omega); \quad \bar{I}_\alpha(\omega) = \frac{\Omega}{2\pi}\int_{t_0}^{t_0+\frac{2\pi}{\Omega}} dt\,[v_\alpha(t,\omega) i_\alpha(t,\omega)]\,, \tag{12}$$

where an average over one modulation cycle is assumed. Moreover, an initial transient t_0 has been discarded to ensure steady state conditions. The transmittances $\mathcal{T}_{1,2}, \mathcal{T}_{2,1}$ are obtained from $\bar{I}_\alpha(\omega)$ in Eq. (12), by setting $V_{\beta'} = 0$, with $\beta' \neq \beta$, and normalizing the incident currents to unit power flux, see inset of Fig. 4a.

In Fig. 4a we compare the thermal radiation for the forward (Fig 1c) and backward (Fig. 1d) configurations, in the absence and presence of spectral filtering $\phi(\omega)$ given by Eq. (10). The currents $\bar{I}_2^{(f/b)}$ are in quantitative agreement with the CMT results. Similarly, the rectification $\mathcal{R}$ for both the unfiltered (open circles) and filtered (filled circles) electronic circuits (Fig. 4c) are in agreement with Eq. (8). We find a linear behavior with Ω (black dashed lines) with the linear coefficient in the case of spectrally engineered baths being two orders larger than the corresponding coefficient found for the unfiltered case.

Conclusion.- We have unveiled the interplay between pumped currents, associated with Floquet driving, and biased currents, associated with the temperature gradient between two reservoirs. When these elements are

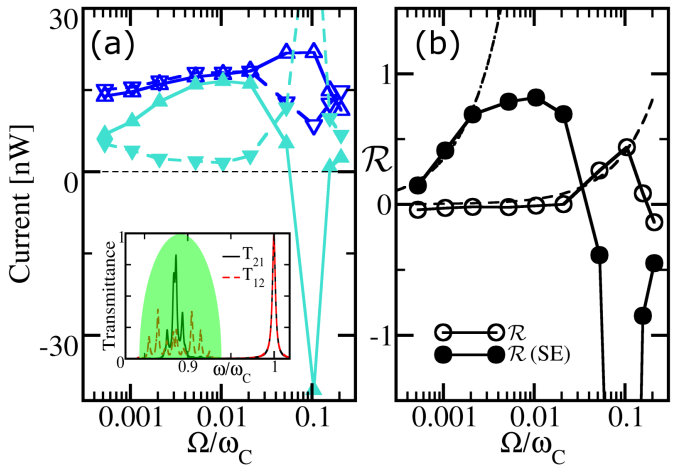

FIG. 4: Time-domain simulations for the electronic circuit of Figs. 1c,d. (a) The radiative currents Eq. (12) vs. Ω are calculated with (filled symbols) and without (open symbols) spectral engineering (SE) for a forward/ backward $\bar{I}_2^{(f/b)}$ configuration. The inset shows the transmission spectrum. (b) The rectification parameter $\mathcal{R}$ vs. Ω. The black dashed lines indicate a function $R = \alpha \times \Omega$ with $\alpha = 4$ and 350 for the unfiltered and filtered circuit respectively. Here $\kappa = 0.1$, $\epsilon = 0.1$, $\delta = 0.05$, $T_{H(C)} = (1 \pm 0.05)T_0$ with $T_0 = 10^9$ K [64] and $\omega_C \approx 0.96\omega_0$.

interlaced with judiciously engineered spectral filters of the reservoirs, they lead to extreme NR thermal radiation. Our results can be used for the design of thermal circulators, and for the identification of efficient refrigeration protocols. It will be interesting to extend this work beyond the limits of applicability of CMT (e.g. spectral window away from the resonance frequencies) using fluctuational electrodynamics methods [36].

Acknowledgements.- (LJFA, TK) acknowledge partial support by an ONR Grant No. N00014-16-1-2803, by an AFOSR Grant No. FA 9550-14-1-0037 and by an NSF Grants No. EFMA-1641109. The postdoctoral work of (HL) at Wesleyan University was supported via grant AFOSR Grant No. FA 9550-14-1-0037. The authors acknowledge Prof. Boris Shapiro for valuable comments.

[1] A. Volokitin and B. Persson, *Near-field radiative heat transfer and noncontact friction*, Rev. Mod. Phys. **79**, 1291 (2007).

[2] J. R. Howell, R. Siegel, and M. P. Mengüs, *Thermal Radiation Heat Transfer*, 5th ed. (CRC Press, Boca Raton, FL, 2010).

[3] T. L. Bergman, A. S. Lavine, F. P. Incropera, and D. P. Dewitt, *Introduction to Heat Transfer*, 6th ed. (Wiley, Hoboken, NJ, 2011).

[4] G. Wehmeyer, T. Yabuki, C. Monachon, J. Wu, C. Dames, *Thermal diodes, regulators, and switches: Physical mechanisms and potential applications*, Appl. Phys. Rev. **4**, 041304 (2017).

[5] S. Fan, *Thermal photonics and energy applications*, Joule **1**, 264 (2017).

[6] W. Li, S. Fan, *Nanophotonic control of thermal radiation for energy applications*, Opt. Express **26**, 15995 (2018).

[7] J. C. Cuevas, F. J. García-Vidal, *Radiative Heat Transfer*, ACS Photonics **5**, 3896 (2018).

[8] D. G. Baranov, Y. Xiao, I. A. Nechepurenko, A. Krasnok, A. Alu, M. A. Kats, *Nanophotonic engineering of far-field thermal emitters*, Nat. Materials **18**, 920 (2019).

[9] G. Kirchhoff, *On the Relation between the Radiating and Absorbing Powers of Different Bodies for Light and heat*, Philos. Mag. Ser 5 **20**, 1 (1860).

[10] L. Zhu and S. Fan, *Near-complete violation of detailed balance in thermal radiation*, Phys. Rev. B **90**, 220301(R) (2014).

[11] Y. Hadad, J. C. Soric, and A. Alú, *Breaking temporal symmetries for emission and absorption*, Proc. Natl. Acad. Sci. U.S.A. **113**, 3471 (2016).

[12] D. A. B. Miller, L. Zhu, and S. Fan, *Universal modal radiation laws for all thermal emitters*, Proc. Natl. Acad. Sci. U.S.A. **114**, 4336 (2017).

[13] J-J Greffet, P. Bouchon, G. Brucoli, F. Marquier, *Light Emission by Nonequilibrium Bodies: Local Kirchhoff Law*, Phys. Rev. X **8**, 021008 (2018).

[14] S. A. Biehs, P. Ben-Abdallah, *Revisiting super-Planckian thermal emission in the far-field regime*, Phys. Rev. B: Condens. Matter Mater. Phys. **93** 165405 (2016).

[15] S. I. Maslovski, C. R. Simovski, S. A. Tretyakov, *Overcoming blackbody radiation limit in free space: metamaterial superemitter*, New J. Phys. **18**, 013034 (2016).

[16] V. Fernández-Hurtado, A. I. Fernández-Domínguez, J. Feist, F. J. García-Vidal, J. C. Cuevas, *Super-Planckian far-field radiative heat transfer*, Phys. Rev. B: Condens. Matter Mater. **97**, 045408 (2018).

[17] V. Fernández-Hurtado, A. I. Fernández-Domínguez, J. Feist, F. J. García-Vidal, J. C. Cuevas, *Exploring the limits of Super-Planckian far-field radiative heat transfer using 2D materials*, ACS Photonics **5**, 3082 (2018).

[18] E. Rephaeli, A. Raman, S. Fan, *Ultrabroadband photonic structures to achieve high-performance daytime radiative cooling*, Nano Lett. **13**, 1457 (2013).

[19] A. P. Raman, M. A. Anoma, L. Zhu, E. Rephaeli, S. Fan, *Passive radiative cooling below ambient air temperature under direct sunlight*, Nature **515**, 540 (2014).

[20] A. R. Gentle, G. B. Smith, *A subambient open roof surface under the mid-summer*, Sun. Adv. Sci. **2**, 1500119 (2015).

[21] J. Kou, Z. Jurado, Z. Chen, S. Fan, A. J. Minnich, *Daytime radiative cooling using near-black infrared emitters*, ACS Photonics **4**, 626 (2017).

[22] Y. Zhai, Y. Ma, S. N. David, D. Zhao, R. Lou, G. Tan, R. Yang, X. Yin, *Scalable-manufactured randomized glass-polymer hybrid metamaterial for daytime radiative cooling*, Science **355**, 1062 (2017).

[23] L. Zhu, A. Raman, K. X. Wang, M. A. Anoma, S. Fan, *Radiative cooling of solar cells*, Optica **1**, 32 (2014).

[24] L. Zhu, A. P. Raman, S. Fan, *Radiative cooling of solar absorbers using a visibly transparent photonic crystal thermal blackbody*, Proc. Natl. Acad. Sci. U. S. A. **112**, 12282 (2015).

[25] W. Li, Y. Shi, K. Chen, L. Zhu, S. Fan, *A comprehensive photonic approach for solar cell cooling* ACS Photonics

4, 774 (2017)

[26] E. Rephaeli, S. Fan, *Absorber and emitter for solar thermo-photovoltaic systems to achieve efficiency exceeding the Shockley-Queisser limit*, Opt. Express **17**, 15145 (2009).

[27] P. Bermel, *et al.*, *Design and global optimization of high-efficiency thermophotovoltaic systems*, Opt. Express **18**, A314 (2010).

[28] M. A. Green, *Time-Asymmetric Photovoltaics*, Nano Lett. **12**, 5985 (2012).

[29] A. Lenert, *et al.*, *A nanophotonic solar thermophotovoltaic device*, Nat. Nanotechnol. **9**, 126 (2015).

[30] I. Latella, A. Pérez-Madrid, J. M. Rubi, S.-A. Biehs, and P. Ben-Abdallah, *Heat Engine Driven by Photon Tunneling in Many-Body Systems*, Phys. Rev. App. **4**, 011001 (2015).

[31] Z. Zhou, E. Sakr, Y. Sun, P. Bermel, *Solar thermophotovoltaics: reshaping the solar spectrum*, Nanophotonics **5**, 1 (2016).

[32] D. M. Bierman, *et al.*, *Enhanced photovoltaic energy conversion using thermally based spectral shaping*, Nat. Energy **1**, 16068 (2016).

[33] A. Fiorino, *et al.*, *Nanogap near-field thermophotovoltaics*, Nat. Nanotechnol. **13**, 806 (2018).

[34] Y. Li, X. Bai, T. Yang, H. Luo, C.-W. Qiu, *Structured thermal surface for radiative camouflage*, Nat. Commun. **9**, 273 (2018).

[35] M. A. Kats, *Vanadium dioxide as a natural disordered metamaterial: perfect thermal emission and large broadband negative differential thermal emittance*, Phys. Rev. X **3**, 041004 (2014).

[36] S. M. Rytov, Y. A. Kravtsov, and V. Tatarskii, *Principles of Statistical Radiophysics* (Springer, Berlin 1989).

[37] H. B. Callen and T. A. Welton, Phys. Rev. 83, 34 (1951).

[38] L. J. Fernández-Alcázar, H. Li, M. Nafari, T. Kottos. *To be published.*

[39] P. Ben-Abdallah, *Photon Thermal Hall Effect*, Phys. Rev. Lett. **116**, 084301 (2016)

[40] A. Ott, R. Messina, P. Ben-Abdallah, S.-A. Biehs, *Radiative thermal diode driven by non-reciprocal surface waves*, Appl. Phys. Lett. **114**, 163105 (2019)

[41] A. Ott, R. Messina, P. Ben-Abdallah, S.-A. Biehs, *Magneto-thermoplasmonics: from theory to applications*, J. Photon. Energy **9**, 032711 (2019)

[42] I. Latella and P. Ben-Abdallah, *Giant Thermal Magnetoresistance in Plasmonic Structures.* Phys. Rev. Lett. **118**, 173902 (2017).

[43] P. Ben-Abdallah, S.-A. Biehs, *Phase-change radiative thermal diode*, Appl. Phys. Lett. **103**, 191907 (2013).

[44] K. Ito, K. Nishikawa, H. Iizuka, and H. Toshiyoshi, *Experimental investigation of radiative thermal rectifier using vanadium dioxide*, Appl. Phys. Lett. **105**, 253503 (2014).

[45] A. Fiorino, D. Thompson, L. Zhu, R. Mittapally, S.-A. Biehs, O. Bezencenet, N. El-Bondry, S. Bansropun, P. Ben-Abdallah, E. Meyhofer, and P. Reddy, *A Thermal Diode Based on Nanoscale Thermal Radiation*, ACS Nano **12**, 5774 (2018).

[46] C. Khandekar, Z. Lin, and A. W. Rodriguez, *Thermal radiation from optically driven Kerr* ($\chi(3)$) *photonic cavities*, Appl. Phys. Lett. **106**, 151109 (2015).

[47] H Li, L. J. Fernández-Alcázar, F. Ellis, B. Shapiro, T. Kottos, *Adiabatic Thermal Radiation Pumps for Thermal Photonics*, Phys. Rev. Lett. **123**, 165901 (2019).

[48] S. Buddhiraju, W. Li , S. Fan, *Photonic Refrigeration from Time-Modulated Thermal Emission*, Phys. Rev. Lett. **124**, 077402 (2020).

[49] I. Latella, R. Messina, J. M. Rubi, P. Ben-Abdallah, *Radiative Heat Shuttling*, Phys. Rev. Lett. **121**, 023903 (2018).

[50] H. Haus, *Electromagnetic Noise and Quantum Optical Measurements* (Springer-Verlag, Berlin, 2000).

[51] L. Zhu, S. Sandhu, C. Otey, S. Fan, M. B. Sinclair, T. S. Luk, *Temporal coupled mode theory for thermal emission from a single thermal emitter supporting either a single mode or an orthogonal set of modes*, Appl. Phys. Lett. **102**, 103104 (2013).

[52] N. Goldman, J. Dalibard, *Periodically driven quantum systems: effective Hamiltonians and engineered gauge fields*, Physical Review X **4**, 031027 (2014).

[53] A. Eckardt and E. Anisimovas, *High-frequency approximation for periodically driven quantum systems from a Floquet-space perspective*, New J. Phys. **17**, 093039 (2015).

[54] A. Eckardt, *Colloquium: Atomic quantum gases in periodically driven optical lattices*, Rev. Mod. Phys. **89**, 011004 (2017).

[55] H. Li, T. Kottos, B. Shapiro, *Floquet-Network Theory of Nonreciprocal Transport*, Phys. Rev. Applied **9**, 044031 (2018).

[56] See supplement for details on presentation of the Floquet Theory of transport (including decimation method), the derivation of energy current in the adiabatic limit, CMT description of electrical circuits, and realistic simulations with whispering gallery mode resonators (including citations to Refs. [65–69]).

[57] H. Li, B. Shapiro, T. Kottos, *Floquet scattering theory based on effective Hamiltonians of driven systems*, Phys. Rev. B **98**, 121101(R) (2018).

[58] H. Li, T. Kottos, *Design Algorithms of Driving-Induced Nonreciprocal Components*, Phys. Rev. Applied **11**, 034017 (2019)

[59] D. L. Sounas, A. Alú, *Non-reciprocal photonics based on time modulation*, Nature Phot. **11**, 774 (2017).

[60] C. Caloz, A. Alú, S. Tretyakov, D. Sounas, K. Achouri, Z.-L. Deck-Léger, *What is Nonreciprocity?*, Phys. Rev. Applied **10**, 047001 (2018).

[61] I. A. D. Williamson, M. Minkov, A. Dutt , J. Wang, A. Y. Song, S. Fan, *Integrated Nonreciprocal Photonic Devices With Dynamic Modulation*, Proc. of the IEEE **108**, 1759 (2020).

[62] I. Datta, S. H. Chae, G. R. Bhatt, M. A. Tadayon, B. Li, Y. Yu, Ch. Park, J. Park, L. Cao, D. N. Basov, J. Hone and M. Lipson, *Low-loss composite photonic platform based on 2D semiconductor monolayers*, Nature Photonics **14**, 256 (2020).

[63] N. Freitas, J.-C. Delvenne, and M. Esposito, *Stochastic and Quantum Thermodynamics of Driven RLC Networks*, Phys. Rev. X **10**, 031005 (2020).

[64] The temperature $T_0 = 10^9$ K can be realized with commercially available noise generators with noise power of $-95 dBm/Hz$.

[65] E. Domany, S. Alexander, D. Bensimon, L.P. Kadanoff, *Solutions to the Schrödinger equation on some fractal lattices*, Phys. Rev. B **28**, 3110 (1983)

[66] H. M. Pastawski and E. Medina, *Tight Binding methods in quantum transport through molecules and small devices: From the coherent to the decoherent description*,

Rev. Mex. Fis. **47S1**, 1 (2001)

[67] C. J. Cattena, L. J. Fernández-Alcázar, R. A. Bustos-Marún, D. Nozaki, and H. M. Pastawski, *Generalized multi-terminal decoherent transport: recursive algorithms and applications to SASER and giant magnetoresistance*, J. Phys.: Condens. Matter **26**, 345304 (2014)

[68] Y. L. Li and P. F. Barker, *Characterization and Testing of a Micro-g Whispering Gallery Mode Optomechanical Accelerometer*, Journal of Lightwave Technology **36**, 3919 (2018).

[69] N. Estep, D. Sounas, J. Soric, A. Alù, *Magnetic-free non-reciprocity and isolation based on parametrically modulated coupled-resonator loops*, Nat. Phys. **10**, 923 (2014)